Kind, R., Sodoudi, F., Yuan, X., Shomali, H., Roberts, R., Gee, D., Eken, T., Bianchi, M., Tilmann, F., Balling, N., Jacobsen, B. H., Kumar, P., Geissler, W. H. (2013): Scandinavia: A former Tibet? - *Geochemistry Geophysics Geosystems (G3)*, *14*, 10, 4479-4487

DOI: 10.1002/ggge.20251

Geochemistry Geophysics Geosystems G3

Article
Volume 14, Number 10
7 October 2013
doi: 10.1002/ggge.20251
ISSN: 1525-2027

Published by AGU and the Geochemical Society

Scandinavia: A former Tibet?

R. Kind and F. Sodoudi
Deutsches GeoForschungsZentrum GFZ, Telegrafenberg, DE-14473 Potsdam, Germany (kind@gfz-potsdam.de)

Freie Universität Berlin, Fachrichtung Geophysik, Berlin, Germany

X. Yuan
Deutsches GeoForschungsZentrum GFZ, Potsdam, Germany

H. Shomali, R. Roberts, and D. Gee
Department of Geophysics, Uppsala University, Uppsala, Sweden

T. Eken and M. Bianchi
Deutsches GeoForschungsZentrum GFZ, Potsdam, Germany

F. Tilmann
Deutsches GeoForschungsZentrum GFZ, Potsdam, Germany

Freie Universität Berlin, Fachrichtung Geophysik, Berlin, Germany

N. Balling and B. H. Jacobsen
Department of Geoscience, Aarhus University, Aarhus, Denmark

P. Kumar
National Geophysical Research Institute NGRI, Hyderabad, Andhra Pradesh, India

W. H. Geissler
Alfred-Wegener-Institut Helmholtz-Zentrum für Polar- und Meeresforschung, Bremerhaven, Germany

[1] The Himalaya and the Tibetan Plateau are uplifted by the ongoing northward underthrusting of the Indian continental lithosphere below Tibet resulting in lithospheric stacking. The layered structure of the Tibetan upper mantle is imaged by seismic methods, most detailed with the receiver function method. Tibet is considered as a place where the development of a future craton is currently under way. Here we study the upper mantle from Germany to northern Sweden with seismic S receiver functions and compare the structure below Scandinavia with that below Tibet. Below Proterozoic Scandinavia, we found two low-velocity zones on top of each other, separated by a high-velocity zone. The top of the upper low-velocity zone at about 100 km depth extends from Germany to Archaean northern Sweden. It agrees with the lithosphere-asthenosphere boundary (LAB) below Germany and Denmark. Below Sweden it is known as the 8°discontinuity, or as a mid-lithospheric discontinuity (MLD), similar to observations in North America. Seismic tomography places the LAB near 200 km in Scandinavia, which is close to the top of our deeper low-velocity zone. We also observed the bottom of the asthenosphere (the Lehmann discontinuity) deepening from 180 km in Germany to 260 km below Sweden. Remnants of old subduction in the upper about 100 km below Scandinavia and Finland are known from controlled source seismic experiments and local earthquake studies. Recent tomographic studies indicate delamination of the lithosphere below southern Scandinavia and northern Germany. We are suggesting that the large-scale layered structure in the Scandinavian upper mantle may be caused by processes similar to the ongoing lithospheric stacking in Tibet.

Components: 6,161 words, 10 figures, 1 table.

Keywords: lithosphere-asthenosphere boundary; remnants of fossil subduction.

Index Terms: 8103 Continental cratons: Tectonophysics; 7218 Lithosphere: Seismology; 1236 Rheology of the lithosphere and mantle: Geodesy and Gravity.

Received 14 May 2013; **Revised** 14 August 2013; **Accepted** 14 August 2013; **Published** 7 October 2013.

Kind, R., et al. (2013), Scandinavia: A former Tibet?, *Geochem. Geophys. Geosyst 14*, 4479–4487, doi:10.1002/ggge.20251

1. Introduction

[2] Cratons are the parts of the continents which have not participated in mantle convection for about a billion years or more and are mostly associated with a thick lithosphere. The mechanisms of their formation are still being debated [see e.g., *Lee et al*., 2011 and references therein for a review]. One of the possibilities is underthrusting and imbrication of lithospheric plates. *Eaton et al*. [2009] have reviewed geophysical observational techniques of the lithosphere-asthenosphere boundary (LAB) and the possibilities to interpret the observations. The contribution of seismology to this question is imaging of structures below the cratons. The S receiver function technique is probably one of the most useful techniques for identifying seismic discontinuities in the upper mantle, especially when low-velocity zones are involved. Particularly, the LAB is observed with this technique in many parts of the world [e.g., *Li et al*., 2004; *Kumar et al*., 2006; *Rychert and Shearer*, 2009; *Rychert et al*., 2010; *Kind and Yuan*, 2010; *Fischer et al*., 2010; *Kumar et al*., 2012].

[3] We are studying the mantle below Scandinavia, the western edge of Baltica, to see if traces of the plate collisions occurring in past geological epochs are still visible. We compare the lithospheric structure of Scandinavia with that of Tibet where continental collision is occurring at present. Northern Europe has a complicated plate tectonic history [e.g., *McKerrow et al*., 2000; see Figure 1]. The last major tectonic events occurred about 400–500 Ma ago when Laurentia, Avalonia, and Baltica collided during the Caledonian orogeny. Dipping mantle reflectors observed in controlled source seismic profiles in several parts of Scandinavia have been interpreted as remnants of fossil subduction [*Balling*, 2000; see Figure 1 for locations]. Seismic discontinuities in the lithospheric mantle observed in Finland have also been interpreted as relicts of ancient subduction and collision processes [*Svekalapko Seismic Tomography Working Group et al*., 2004; see Figure 1 for locations]. These observations indicate that such structures can survive a very long time [*Balling*, 2000]. Recently, *Zhu et al*. [2012a, 2012b] found indications of southward directed lithospheric delamination below southern Scandinavia and northern Germany in seismic tomography.

2. Data and Method

[4] The data we used comprise teleseismic observations recorded at 95 permanent and temporary broadband stations in Germany, Denmark, Sweden, and Finland (Figure 2 and Table 1). The S receiver function technique was used rather than the

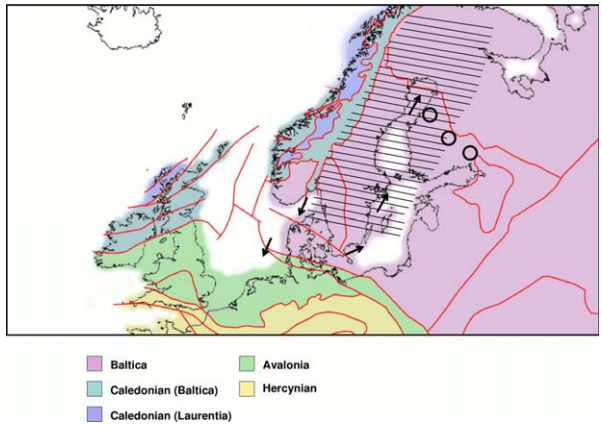

Figure 1. Tectonic structure of northern Europe (see e.g., *McKerrow et al*. [2000]; map modified from *Woudloper* [2013]). The hatched area marks the region where we have observed layering in the lithosphere. Arrows indicate location and dip direction of mantle reflectors which are observed in controlled source profiles [*Balling*, 2000]. Circles indicate mantle reflectors near 100 km depth observed in local earthquake records [*Svekalapko Seismic Tomography Working Group et al*., 2004].

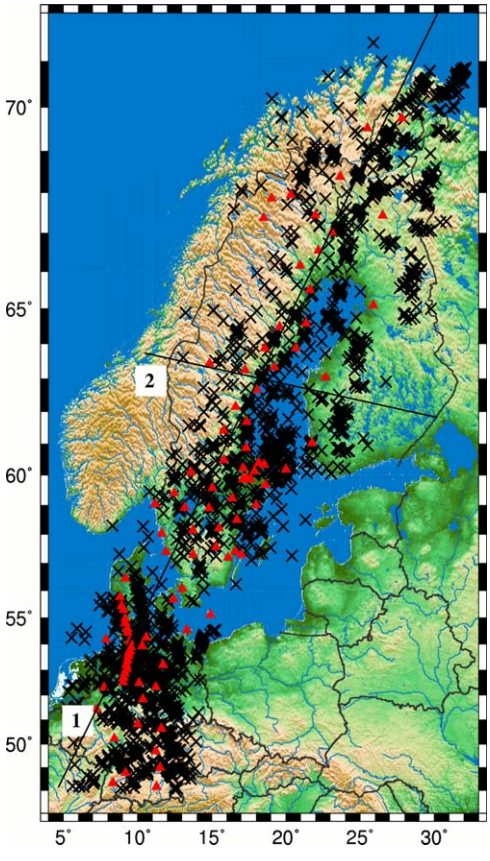

Figure 2. Map of all seismic broadband stations used (red triangles). Station names and coordinates can be found in Table 1. Most data come from the Swedish National Seismic Network (SNSN, http://snsn.geofys.uu.se/) (1 year data used). The dense line of red triangles marks the temporary JULS experiment (2 years deployment). Black crosses mark piercing points of S-to-P converted waves at 100 km depth using the IASP91 model [*Kennett and Engdahl*, 1991]. The two lines 1 and 2 mark the profiles onto which the data are projected.

P receiver function technique because crustal multiples are completely separated from direct conversions in S receiver functions. In P receiver functions such multiples may cover direct conversions or may be misinterpreted as direct conversions [*Kind et al.*, 2012]. We searched visually through the S signals of records from earthquakes with magnitudes greater 5.7 (Figure 3). A first rotation of the components was carried out using theoretical back azimuth and incidence angles. We have selected broadband events with signal-to-noise ratios greater than about 5 (ratio between the S arrival on the SV component to the noise on the P component in front of the SV arrival). We only accepted signals with simple waveforms on the SV component, meaning one or two swings in the broadband waveforms. We obtained finally about

Table 1. Coordinates of Seismic Stations Used in Our Study and Archives Which Supplied the Data[a]

	Code	LAT	LON	Network	Archive
1	KEV	69.755	27.806	IU	IRIS
2	ARE0	69.534	25.505	NO	ORFEUS
3	HEF	68.391	23.657	HE	GEOFON
4	KUR	67.954	20.337	SNSN	UPP
5	NIK	67.867	19.035	SNSN	UPP
6	MAS	67.457	21.998	SNSN	UPP
7	SGF	67.442	26.526	FN	GEOFON
8	SAL	67.380	18.507	SNSN	UPP
9	PAJ	67.024	23.113	SNSN	UPP
10	ERT	66.554	22.190	SNSN	UPP
11	HAR	66.163	20.975	SNSN	UPP
12	SJU	65.508	21.605	SNSN	UPP
13	OUL	65.085	25.896	FN	GEOFON
14	BUR	64.584	21.377	SNSN	UPP
15	SVA	64.494	19.575	SNSN	UPP
16	BRE	63.891	18.578	SNSN	UPP
17	UMA	63.883	20.678	SNSN	UPP
18	NOR	63.443	14.857	SNSN	UPP
19	HUS	63.342	19.218	SNSN	UPP
20	SOL	63.247	17.258	SNSN	UPP
21	VAF	63.042	22.671	HE	GEOFON
22	HEM	62.676	18.036	SNSN	UPP
23	HAS	62.153	16.614	SNSN	UPP
24	ARN	61.692	17.378	SNSN	UPP
25	ROT	61.420	15.814	SNSN	UPP
26	RAF	61.022	21.767	SNSN	UPP
27	IGG	60.873	17.316	SNSN	UPP
28	FAL	60.494	15.832	SNSN	UPP
29	FOR	60.387	18.180	SNSN	UPP
30	GRA	60.334	18.540	SNSN	UPP
31	OST	60.230	17.134	SNSN	UPP
32	AAL	60.178	19.994	SNSN	UPP
33	FLY	60.128	17.885	SNSN	UPP
34	UDD	60.090	13.607	SNSN	UPP
35	FIB	59.901	17.352	SNSN	UPP
36	UP1	59.858	17.627	SNSN	UPP
37	BAC	59.854	17.108	SNSN	UPP
38	NRT	59.677	18.631	SNSN	UPP
39	NRA	59.570	15.040	SNSN	UPP
40	FIN	59.403	12.479	SNSN	UPP
41	ESK	59.231	16.394	SNSN	UPP
42	STR	59.035	11.182	SNSN	UPP
43	NYN	59.005	18.004	SNSN	UPP
44	NAS	58.928	13.186	SNSN	UPP
45	ASK	58.895	14.829	SNSN	UPP
46	VIK	58.502	16.699	SNSN	UPP
47	LNK	58.223	15.505	SNSN	UPP
48	FKP	58.159	13.724	SNSN	UPP
49	TJO	58.032	11.625	SNSN	UPP
50	EKS	57.573	15.302	SNSN	UPP
51	ASP	57.418	16.599	SNSN	UPP
52	ONS	57.397	11.926	SNSN	UPP
53	GNO	57.290	13.756	SNSN	UPP
54	BYX	57.290	17.008	SNSN	UPP
55	OSK	57.195	16.099	SNSN	UPP
56	MUD	56.455	9.173	DK	GEOFON
57	BJU	56.074	13.023	SNSN	UPP
58	J04B	55.772	8.829	JULS	
59	COP	55.685	12.432	DK	GEOFON
60	J06B	55.451	8.938	JULS	GEOFON
61	J07B	55.308	9.062	JULS	GEOFON
62	BSD	55.113	14.914	DK	GEOFON
63	J09B	54.972	9.173	JULS	GEOFON
64	J10B	54.814	9.174	JULS	GEOFON
65	J11S	54.602	9.311	JULS	GEOFON
66	RGN	54.547	13.321	GE	GEOFON

Table 1. (continued)

	Code	LAT	LON	Network	Archive
67	J12B	54.442	9.354	JULS	GEOFON
68	J0CB	54.261	10.591	JULS	GEOFON
69	HLG	54.184	7.883	GE	GEOFON
70	J14S	54.113	9.465	JULS	GEOFON
71	J15B	53.901	9.559	JULS	GEOFON
72	J16B	53.733	9.493	JULS	GEOFON
73	J25B	53.666	9.402	JULS	GEOFON
74	J17B	53.556	9.399	JULS	GEOFON
75	J18B	53.392	9.337	JULS	GEOFON
76	J19B	53.204	9.248	JULS	GEOFON
77	J20B	53.054	9.290	JULS	GEOFON
78	J21B	52.872	9.138	JULS	GEOFON
79	J22B	52.702	9.072	JULS	GEOFON
80	J23B	52.536	9.300	JULS	GEOFON
81	BSEG	53.935	10.316	GR	BGR
82	J0DB	53.208	11.715	JULS	GEOFON
83	NRDL	52.494	10.107	GR	BGR
84	FLT1	52.330	11.237	GE	GEOFON
85	IBBN	52.306	7.759	GE	GEOFON
86	CLZ	51.842	10.372	GR	BGR
87	BUG	51.441	7.269	GR	BGR
88	UBBA	50.819	10.001	GR	BGR
89	MOX	50.645	11.616	GR	BGR
90	TNS	50.222	8.447	GR	BGR
91	GRA1	49.692	11.222	GR	BGR
92	GRC1	48.996	11.521	GR	BGR
93	STU	48.771	9.193	GE	GEOFON
94	BFO	48.330	8.330	GR	BGR
95	FUR	48.163	11.275	GR	BGR

[a]BGR: Bundesanstalt für Geowissenschaften und Rohstoffe, Hannover, Germany, http://www.bgr.bund.de/; GEOFON: International Seismic Network, Archive at GFZ Potsdam, Germany, http://geofon.gfz-potsdam.de/; SNSN: Swedish National Seismic Network, Uppsala University, Sweden, http://snsn.geofys.uu.se/; IRIS: Incorporated Research Institution for Seismology, Seattle, USA, http://www.iris.edu/; and ORFEUS: Observatories and Research Facilities for European Seismology, De Bilt, Netherlands, http://www.orfeus-eu.org/

3300 traces. A second rotation of the components was carried out with the selected traces by choosing those rotation angles which led to the least energy on the P component at the time of the signal maximum on the SV component. After this, the P components were deconvolved by the SV components, migrated into the depth domain or moveout corrected and summed in time domain. Depth migration consists of back projection according to Snell's law and summation of the incoming rays within the Fresnel zone. For migration, the global reference model IASP91 was used [*Kennett and Engdahl*, 1991]. Since the upper mantle below Denmark and Germany is about 4% slower than below Sweden [e.g., *Zhu et al.*, 2012a; *Gregersen et al.*, 2010] down to 300 km depth, the use of a homogeneous model for migration may result in a systematic depth bias of mantle discontinuities of the same percentage. We have also experimented with the "plain summation" technique [*Kumar et al.*, 2010], in which summation is performed without previous deconvolution, since deconvolution may alter the response of the receiver site [*Kumar et al.*, 2010]. We found no significant differences of both techniques, except that the deconvolution resulted in a better signal-to-noise ratio. Therefore, we used deconvolution.

[5] The observed seismic data are shown in time domain in Figure 4 and in depth migrated form in Figure 5. It should be kept in mind that the colors in Figure 5 do not indicate volumetric structures as in tomographic images but seismic discontinuities. Red (blue) signals mark S-to-P converted waves at a seismic discontinuity with downward increasing (decreasing) velocities. Amplitudes of the converted seismic signals permit in general measurements of velocity ratios at the discontinuities. However, we have avoided interpreting amplitudes quantitatively because of relatively strong small-scale lateral inhomogeneities in the upper mantle and which would make estimates of the reliability of the resulting velocity ratios difficult. To judge the reliability of our data in general we compare Figures 4 and 5. These figures result from different processing methods but still show the same marked seismic phases. The reliability of the data can also be seen in the large-scale similarity of neighboring summation traces in Figure 4. Neighboring summation traces do not have a single trace in common, no lateral smoothing is applied. That means that seismic phases which correlate over several summation traces are a clear indication of geological structure inside the Earth and not noise. During the processing we have also done

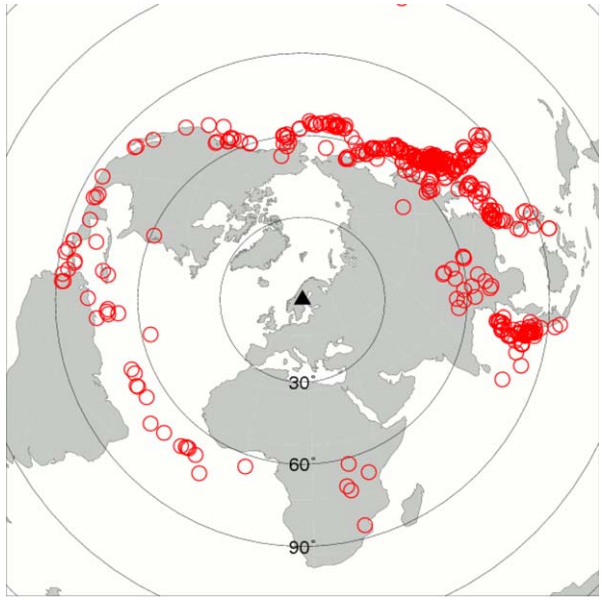

Figure 3. Map of epicenters of all events used.

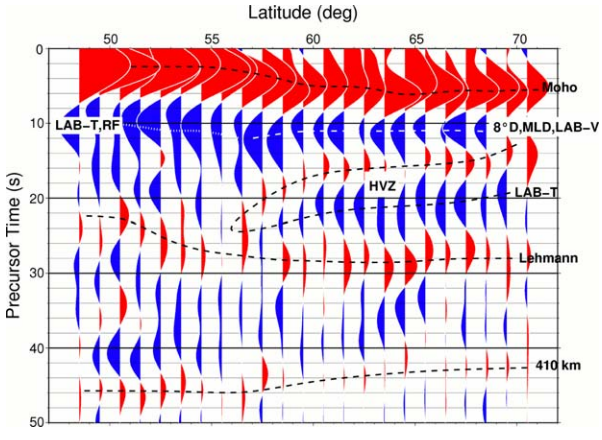

Figure 4. Summation plots of all available S receiver functions (*P* wave component) taken along the south-north profile 1 (Figure 2). Zero time is the arrival of the S waves on the SV component (which is not shown). Time scale marks the arrival time ahead of the S wave. Dashed lines mark laterally coherent converted seismic phases. All traces with piercing points at 100 km depth within a latitude window of 1° (without overlap) are summed. The number of summed traces varies between 60 and 250 for each window. All traces are moveout corrected before summation with a reference slowness of 6.4 s/°. A low-pass filter with 8 s cutoff period was applied. The marks at the seismic signals have the following meaning: Moho = crust mantle boundary, LAB-T, RF = lithosphere-asthenosphere boundary observed with seismic tomography and receiver functions, LAB-T = LAB observed so far only with tomography, LAB-V = LAB modeled from post glacial rebound data, MLD = mid-lithospheric discontinuity observed with receiver functions and surface wave tomography, and 8°D = low-velocity zone observed with controlled source seismic experiments.

bootstrapping tests, which confirmed the robustness of the marked discontinuities.

3. Results

[6] The stacks in Figures 4 and 5 show a number of laterally coherent seismic phases. The Moho is the most prominent signal and shows the known depth increase [e.g., *Gossler et al.*, 1999; *Alinaghi et al.*, 2003; *Medhus et al.*, 2012] from central Europe to Scandinavia. A shorter period plot of the Moho with greater depth resolution is shown in Figure 6. In Figures 4, 5 and 7, we observe directly below the Moho a continuous negative signal (blue, marked MLD, LAB-V, 8°D in the north and LAB-T, RF in the south) over a length of more than 2000 km, crossing several tectonic provinces. Below Proterozoic Sweden, we observe the positive (red) top and the negative (blue) bottom of a high-velocity structure extending over more than 1200 km (marked "HVZ"). The red (positive) signal marked "Lehmann" is likely the bottom of the asthenosphere. It was discussed by *Lehmann* [1964] and is assumed frequently to be a global feature. The Lehmann discontinuity is relatively rarely well observed. The global reference model PREM [*Dziewonski and Anderson*, 1981] contains such a feature at 220 km depth, whereas the IASP91 global reference model does not contain it. Here we have a clear signal over 2000 km length at approximately the expected depth range, which is, however, not constant but deepening from 180 km in Germany to 260 km below Sweden.

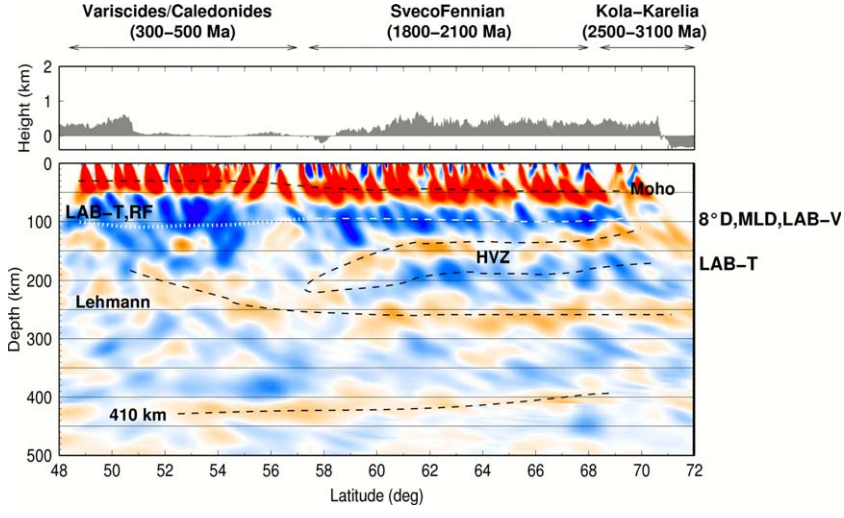

Figure 5. The same S receiver function data as in Figure 4 migrated into depth using the IASP91 model and projected on the south-north profile 1 in Figure 2. The same discontinuities identified in Figure 4 are also clearly visible in this figure. The same phase marks as in Figure 4 are used. (top) Topography along the profile.

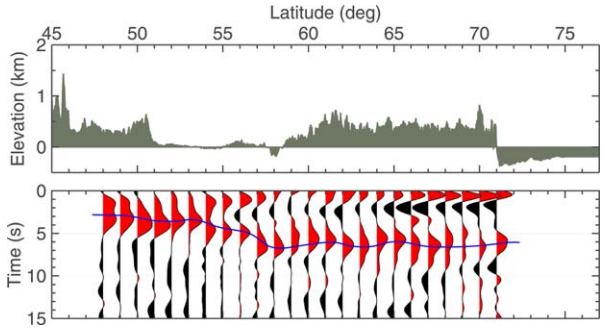

Figure 6. One second low pass filtered S receiver function image of the Moho (blue line) along the south-north profile. Window size is 2°, moved by 1°, piercing point depth is 50 km. Note that in this period band no continuous negative discontinuity at 9–12 s precursor time is visible like in Figure 4. This means that the negative discontinuity is not as sharp as the Moho or more scattered, or both. Note that the filtering did not produce significant side lobes of the Moho signal.

[7] We would like to point out another possible observation in the data. Above the 410 discontinuity, we note a cluster of blue signals especially in the southern end of the profile below Denmark and Germany. There are a number of other observations about similar low-velocity structures above the 410 in several parts in the world, for example in northwestern Canada [see *Schaeffer and Bostock*, 2010, and references therein]. It is interpreted as a zone of partial melt. Perhaps our observations have a similar origin.

[8] The known seismic discontinuity at 410 km global reference depth (IASP91) [*Kennett and Engdahl*, 1991] is also visible. Its apparent shallowing from central Europe to Scandinavia is probably due to the faster seismic velocities in the Scandinavian upper mantle. The observation of the established discontinuities at the crust-mantle boundary (Moho) and at 410 km depth is also serving as a confirmation of the correctness of our imaging technique.

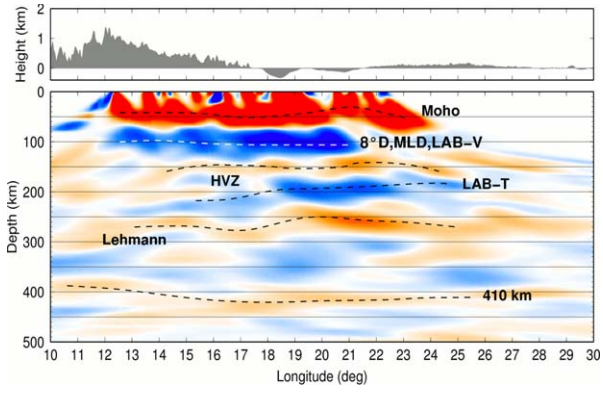

Figure 7. Migrated 500 km wide profile of S receiver functions along the west-east profile 2 in Figure 2 (all parameters and marks as in Figure 5).

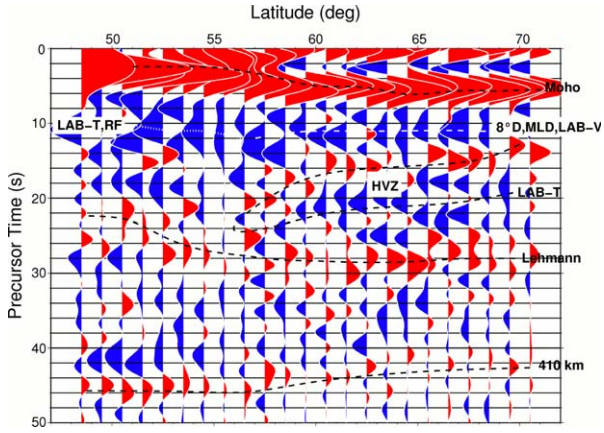

Figure 8. Same data as in Figure 4 but filtered with a 4 s low-pass filter. Marks are taken from Figure 4. This figure shows that the discontinuities (except the Moho) appear laterally homogeneous only in the longer period data.

4. Discussion

4.1. Comparison with Previous Lithospheric Thickness Estimates in Fennoscandia

[9] An earlier S receiver function study also based on data from the Swedish network [*Olsson et al.*, 2007] found, in agreement with our results, a large-scale negative discontinuity at 200 km which they interpreted as LAB (named L in their Figure 6). Over a shorter distance range they found also a negative discontinuity near 100 km depth (named B in their Figure 6). *Olsson et al.* [2007] infer an additional negative discontinuity near 160 km depth (named D1 and D2 in their Figure 6), which we do not observe. The main reason for this difference is probably that we used a longer period low-pass filter (8 s corner period). For comparison, we have plotted in Figures 8 and 9 shorter period filtered data (4 s corner period). In these figures, the observed phases appear much more scattered. This could be interpreted that the mantle discontinuities are laterally much more heterogeneous than, for example, the Moho and that only longer period seismic waves smooth over small-scale variability of the internal boundaries. Such small-scale lateral inhomogeneities would also cause a problem for interpreting the amplitudes of the converted waves in summation traces. Alternatively, the lower signal-to-noise ratio of the shorter-period receiver

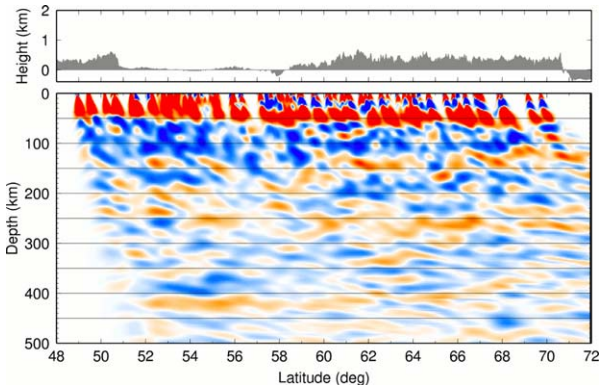

Figure 9. Shorter period filtered (4 s low pass) version of the data in Figure 5.

functions results in a more scattered appearance. What can be said is that the velocity contrast of the mantle discontinuities is approximately only about half the size of the contrast at the Moho, as an amplitude comparison in Figure 4 shows.

[10] From seismic tomography it is known that the lithosphere below the Baltic Shield is thicker than below Phanerozoic Europe [*Legendre et al*., 2012; *Zhu et al*., 2012a, 2012b] as well as from regional studies in Sweden and Denmark [*Shomali et al*., 2002; *Gregersen et al*., 2010; *Eken et al*., 2012; *Medhus et al*., 2012; *Wawerzinek et al*., 2012]. Similar contrasts in lithospheric thickness were inferred from a European-scale receiver function study [*Geissler et al*., 2010] and depth dependence of seismic anisotropy [*Plomerova and Babuška*, 2010]. These results are also reflected in our data in the phase marked LAB-T in Figures 4 and 5, which is in Scandinavia the bottom of the zone marked HVZ. A low-velocity zone at about 100–140 km depth (8°D) in Scandinavia has previously been observed in controlled source seismic data and interpreted as caused by partial melt or grain-boundary sliding [*Thybo*, 2006; *Artemieva and Thybo*, 2008; *Karato*, 2012]. Our data confirm also the existence of this low-velocity zone. It appears at a similar depth as the LAB in Phanerozoic Europe (LAB-T, RF) in Figures 4 and 5.

[11] The original definition of the lithosphere-asthenosphere system came from post glacial rebound observations [*Barrell*, 1914]. Recent modeling of GPS displacement data of the ongoing post-glacial rebound in Scandinavia resulted in layered viscosity upper mantle models with a lithospheric thickness near 100 km [*Zhao et al*., 2012, and references therein]. Intriguingly, this is a similar depth range as the 8°discontinuity seen in controlled source data and the upper low-velocity zone in our S receiver function data (LAB-V), and represents a much lower lithospheric thickness estimate than the 200 km thickness obtained from tomography and the deeper low-velocity zone in our data (LAB-T).

4.2. Observations in Other Cratons

[12] A comparison of our receiver function results below Scandinavia with similar data below the North American craton shows significant similarities. S and P receiver functions show a negative discontinuity near 100 km in the entire US, including in the cratonic central and eastern US [*Rychert and Shearer*, 2009; *Kumar et al*., 2012]. This observation is very similar to our results for Scandinavia. Tomography techniques find the lithosphere extending to about 200 km depth in the cratonic US and weak indications for a low-velocity zone near 100 km [*Yuan and Romanowicz*, 2010]. The negative discontinuity near 100 km is named mid-lithospheric discontinuity (MLD) [*Lekic and Romanowicz*, 2011] outside the western US, caused perhaps by grain-boundary sliding [*Karato*, 2012] or anisotropy. In the Canadian Shield indications of remnant subduction have been observed in receiver functions and controlled source seismic data [*Bostock*, 1997, 1998]. Mid-lithospheric discontinuities have been observed at several locations beneath the Canadian Shield and interpreted as remnants of slabs of Proterozoic age [*Miller and Eaton*, 2010] but the depth of the MLDs observed by them is more variable than we find below Scandinavia. Nevertheless, their interpretation highlights the possibility of structural interpretations of the MLD, in contrast to the earlier interpretation in terms of petrology. Layering of the cratonic mantle is also observed in South Africa [*Sodoudi et al*., 2013] where a shallow MLD at ~85 km depth was interpreted in terms of anisotropy, and a deeper MLD at ~150–200 km in terms of a compositional boundary.

[13] Tibet has a very young geological history compared with typical cratons; however, it is considered a future craton by *McKenzie and Priestley* [2008]. The layered structure of the Tibetan mantle is imaged with high resolution and related to the ongoing collision of India with Eurasia (see Figure 10). The subducting Indian plate is directly visible in tomography and receiver function images [e.g., *Li et al*., 2008; *Zhao et al*., 2011]. Besides the generally accepted Indian continental subduction below Tibet, there might also exist, at least in some regions, Eurasian subduction from the north below Tibet. Therefore, in central Tibet two lithospheres are probably stacked on top of each other [*Zhao et al*., 2011]. The image of the Tibetan layered upper

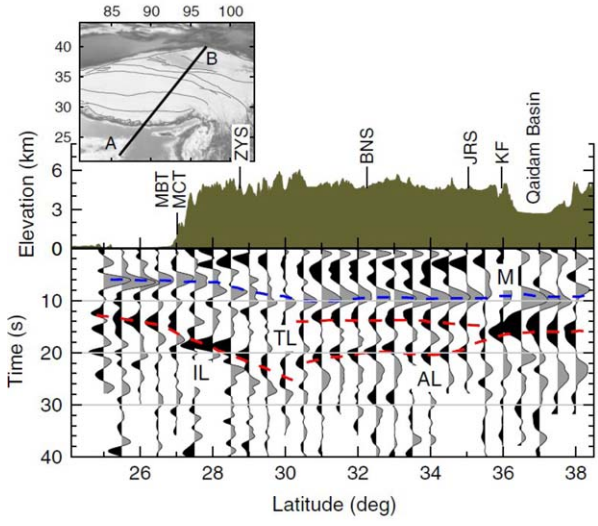

Figure 10. S receiver function section across Tibet. Moho (M) and several negative phases below the Moho are visible. The negative phases are interpreted as bottom of the north subducting Indian lithosphere (IL) in the south, as bottom of the south subducting Asian lithosphere (AL) in the north and as bottom of a Tibetan lithosphere (TL) overriding the Asian lithosphere in the central part of Tibet. (top) The profile along which the above section has been obtained (from *Kind et al*. [2012] after *Zhao et al*. [2011]).

mantle appears very similar to the image of the Scandinavian layered upper mantle. The Indian mantle lithosphere is penetrating up to 500 km to the north below Tibet over a frontal length of about 1500 km. Our observations of a layering beneath Scandinavia cover a region of almost comparable size, about 1000 km times several 100 km. However, the layering is observed within the Baltica block, so if the layering in Scandinavia is collision-related, it probably originates from pre-Caledonian events for which no clear subduction geometries can be discerned. So, different from Tibet, there is no clear indication what other lithosphere is underthrusting in Scandinavia and when exactly this happened. Nevertheless, similar to the North American cratons, the structures observed by us provide evidence that traces of collision processes are retained within the mantle lithosphere for a very long time.

5. Conclusion

[14] Our main observations are the large-scale layered structure of the Scandinavian upper mantle, which appears very similar to that of the Tibetan upper mantle. In Tibet, we have clear evidence that mainly underthrusting of the Indian plate is causing this layering. Comparable evidence for the origin of layering in Scandinavia is still missing. Inclined structures in the upper mantle below cratons have been known for a long time and have been interpreted as remnants of fossil subduction. It is still an open question how these structures could survive such a long time. They are a confirmation of those underthrusting events which may have contributed to craton building, as discussed, for example, in the review by *Lee et al*. [2011]. Our data have considerably expanded the observations of the layered structure of the Scandinavian craton. We conclude that the tectonic event (or perhaps several events) that possibly led to the layering of the Scandinavian upper mantle must have been of comparable significance as the recent collision of India and Eurasia. It is still difficult to model details realistically since not yet enough data are available for a full three-dimensional picture. To achieve this, more data from the edges of Baltica, especially Norway, Finland, Denmark, and northern Germany are needed. Most of our data are aligned along a south-north profile which is likely along the strike direction of the main Caledonian collision. More data for profiles of sufficient length perpendicular to this strike direction are necessary for the identification of the specific underthrusting processes.

Acknowledgments

[15] We wish to thank the Deutsche Forschungsgemeinschaft for their support. T.E. was supported by a fellowship of the Alexander-von-Humboldt foundation. We also thank all data collectors and distributors which are listed in the caption of Table 1. We also like to thank the editor and two reviewers for their helpful comments.

References

Alinaghi, A., G. Bock, R. Kind, W. Hanka, and K. Wylegalla (2003), Receiver function analysis of the crust and upper mantle from the North German Basin to the Archaean Baltic Shield, *Geophys. J. Int.*, *155*, 641–652.

Artemieva, I. M., and H. Thybo (2008), Deep Norden: Highlights of the lithospheric structure of Northern Europe, *Iceland, and Greenland, Episodes*, *31*(1), 98–106.

Balling, N. (2000), Deep seismic reflection evidence for ancient subduction and collision zones within the continental lithosphere of northwestern Europe, *Tectonophysics*, *329*, 269–300.

Barrell, J. (1914), The strength of the Earth's crust, *J. Geol.*, *22*, 655–683.

Bostock, M. G. (1997), Anisotropic upper-mantle stratigraphy and architecture of the Slave craton, *Nature*, *390*, 392–395.

Bostock, M. G. (1998), Mantle stratigraphy and evolution of the Slave province, *J. Geophys. Res.*, *103*(B9), 21,183–21,200.

Dziewonski, A. M., and D. L. Anderson (1981) Preliminary reference Earth model, *Phys. Earth Planet. Inter.*, *25*, 297–356.

Eaton, D. W., F. Darbyshire, R. L. Evans, H. Grütter, A. G. Jones, and X. Yuan (2009), The elusive lithosphere-asthenosphere boundary (LAB) beneath cratons, *Lithos*, *109*(1–2), 1–22, doi.org/10.1016/j.lithos.2008.05.009.

Eken, T, J. Plomerova, L. Vecsey, V. Babuska, R. Roberts, H. Shomali, and R. Bödvarsson (2012), Effects of seismic anisotropy on P-velocity tomography of the Baltic Shield, *Geophys. J. Int.*, *188*, 600–612.

Fischer, K. M., H. A. Ford, D. L. Abt, and C. A. Rychert (2010), The lithosphere-asthenosphere boundary, *Annu. Rev. Earth Planet. Sci.*, *38*, 551–575, doi:10.1146/annurev-earth-040809-152438.

Geissler, W. H., F. Sodoudi, and R. Kind (2010), Thickness of the central and eastern European lithosphere as seen by S receiver functions, *Geophys. J. Int.*, *181*, 604–634.

Gossler, J., R. Kind, S. V. Sobolev, H. Kämpf, K. Wylegalla, M. Stiller, and TOR Working Group (1999), Major crustal features between the Harz Mountains and the Baltic Shield derived from receiver functions, *Tectonophysics*, *314*, 321–333.

Gregersen, S., P. Voss, S. V. Nielsen, U. Achauer, A. Busche, W. Rabbel, and Z. H. Shomali (2010), Uniqueness of modeling results from teleseismic P-Wave tomography in Project Tor, *Tectonophysics*, *481*, 99–107.

Karato, S. (2012), On the origin of the asthenosphere, *Earth Planet. Sci. Lett.*, *321–322*, 95–103.

Kennett, B. L. N., and E. R. Engdahl (1991), Travel times for global earthquake location and phase identification, *Geophys. J. Int.*, *105*(2), 429–465.

Kind, R., and X. H. Yuan (2010), Seismic images of the biggest crash on Earth, *Science*, *329*, 1479–1480.

Kind, R., X. Yuan, and P. Kumar (2012), Seismic receiver functions and the lithosphere-asthenosphere boundary, *Tectonophysics*, *536–537*, 25–43.

Kumar, P., R. Kind, and X. Yuan (2010), Receiver function summation without deconvolution, *Geophys. J. Int.*, *180*, 1223–1230.

Kumar, P., X. Yuan, R. Kind, and J. Ni (2006), Imaging the colliding Indian and Asian lithospheric plates beneath Tibet, *J. Geophys. Res.*, *111*, B06308, doi:10.1029/2005JB003930.

Kumar, P., X. Yuan, R. Kind, and J. Mechie (2012), The lithosphere-asthenosphere boundary observed with USArray receiver functions, *Solid Earth*, *3*, 149–159.

Lee, C.-T. A., P. Luffi, and E. J. Chin (2011), Building and destroying continental mantle, *Annu. Rev. Earth Planet. Sci.*, *39*, 59–90, doi:10.1146/annurev-earth-040610–133505.

Legendre, C. P., T. Meier, S. Lebedev, W. Friederich, and L. Viereck-Götte (2012), A shear wave velocity model of the European upper mantle from automated inversion of seismic shear and surface waveforms, *Geophys. J. Int.*, *191*, 282–304.

Lehmann, I. (1964), On the velocity of P in the upper mantle, *Bull. Seismol. Soc. Am.*, *54*, 1097–1103.

Lekic, V., and B. Romanowicz (2011), Tectonic regionalization without a priori information: A cluster analysis of upper mantle tomography, *Earth Planet. Sci. Lett.*, *308*, 151–160, doi:10.1016/j.epsl.2011.05.050.

Li, X., R. Kind, X. H. Yuan, I. Wolbern, and W. Hanka (2004), Rejuvenation of the lithosphere by the Hawaiian plume, *Nature*, *427*, 827–829, doi:10.1038/nature02349.

Li, C., R. D. van der Hilst, A. S. Meltzer, and E. R. Engdahl (2008), Subduction of the Indian lithosphere beneath the Tibetan Plateau and Burma, *Earth Planet. Sci. Lett.*, *274*, 157–168.

McKenzie, D., and K. Priestley (2008), The influence of lithospheric thickness variations on continental evolution, *Lithos*, *102*, 1–11.

McKerrow, W. S., C. Mac Niocaill, and J. F. Dewey (2000), The Caledonian Orogeny redefined, *J. Geol. Soc.*, *157*, 1149–1154.

Medhus, A. B., N. Balling, B. H. Jacobsen, C. Weidle, R. W. England, R. Kind, H. Thybo, and P. Voss (2012), Uppermantle structure beneath the Southern Scandes Mountains and the Northern Tornquist Zone revealed by P-wave, *Geophys. J. Int.*, *189*, 1315–1334, doi:10.1111/j.1365-246X.2012.05449.x.

Miller, M. S., and D. W. Eaton (2010), Formation of cratonic mantle keels by arc accretion: Evidence from S receiver functions, *Geophys. Res. Lett.*, *37*, L18305, doi:10.1029/2010GL044366.

Olsson, S., R. G. Roberts, and R. Bödvarsson (2007), Analysis of waves converted from S to P in the upper mantle beneath the Baltic Shield, *Earth Planet. Sci. Lett.*, *257*, 37–46.

Plomerova, J., and V. Babuška (2010), Long memory of mantle lithosphere fabric-European LAB constrained from seismic anisotropy, *Lithos*, *120*, 131–143.

Rychert, C. A., and P. M. Shearer (2009), A global view of the lithosphere-asthenosphere boundary, *Science*, *324*, 495–498.

Rychert, C. A., P. M. Shearer, and K. M. Fischer (2010), Scattered wave imaging of the lithosphere asthenosphere boundary, *Lithos*, *120*, 173–185.

Schaeffer, A. J., and M. G. Bostock (2010), A low-velocity zone atop the transition zone in northwestern Canada, *J. Geophys. Res.*, *115*, B06302, doi:10.1029/2009JB006856.

Shomali, Z. H., R. G. Roberts, and Tor Working Group (2002), Non-linear body wave teleseismic tomography along the TOR array, *Geophys. J. Int.*, *148*, 562–574.

Sodoudi, F., R. Kind, and E. Kaestle, (2013), Imaging the LAB and other lithospheric discontinuities beneath South Africa, *Geophys. Res. Abstr.*, *15*, EGU2013–3237-2.

Svekalapko Seismic Tomography Working Group, J. Yliniemi, E. Kozlovskaya, S. E. Hjelt, A. Komminaho, and A. Ushakov (2004), Structure of the crust and uppermost mantle beneath southern Finland revealed by analysis of local events registered by the SVEKALAPKO seismic array, *Tectonophysics*, *394*, 41–67.

Thybo, H. (2006), The heterogeneous upper mantle low velocity zone, *Tectonophysics*, *416*(1–2), 53–79.

Wawerzinek, B., J. R. R. Ritter, and C. Roy (2012), New constraints on the 3D shear wave velocity structure of the upper mantle underneath Southern Scandinavia revealed from nonlinear tomography, *Tectonophysics*, *602*(2013), 38–54, doi:10.1016/j.tecto.2012.12.033.

Woudloper (2013), [Available at http://en.wikipedia.org/wiki/File:Tectonic_map_Europe.jpg.].

Yuan, H., and B. Romanowicz (2010), Lithospheric layering in the North American craton, *Nature*, *466*, 1063–1069.

Zhao, W., et al. (2011), Tibetan plate overriding the Asian plate in central and northern Tibet, *Nat. Geosci.*, *4*, 870–873.

Zhao, S., K. Lambeck, and M. Lidberg (2012), Lithosphere thickness and mantle viscosity inverted from GPS-derived deformation rates in Fennoscandia, *Geophys. J. Int.*, *190*, 278–292, doi:10.1111/j.1365-246X.2012.05454.x.

Zhu, H., E. Bozdag, D. Peter, and J. Tromp (2012a), Seismic wavespeed images across the Iapetus and Tornquist suture zones, *Geophys. Res. Lett.*, *39*, L18304, doi:10.1029/2012GL053053.

Zhu, H., E. Bozdag, D. Peter, and J. Tromp (2012b), Structure of the European upper mantle revealed by adjoint tomography, *Nat. Geosci.*, *5*, 493–498, doi:10.1038/NGEO1501.